JCB Article

Mice lacking JunB are osteopenic due to cell-autonomous osteoblast and osteoclast defects

Lukas Kenner,[1] Astrid Hoebertz,[1] Timo Beil,[2] Niamh Keon,[3] Florian Karreth,[1] Robert Eferl,[1] Harald Scheuch,[1] Agnieszka Szremska,[1] Michael Amling,[2] Marina Schorpp-Kistner,[3] Peter Angel,[3] and Erwin F. Wagner[1]

[1]Research Institute of Molecular Pathology (IMP), A-1030 Vienna, Austria
[2]Department of Trauma, Hand, and Reconstructive Surgery, Hamburg University School of Medicine, D-20246 Hamburg, Germany
[3]Department of Signal Transduction and Growth Control, Deutsches Krebsforschungszentrum (DKFZ), D-69120 Heidelberg, Germany

Because JunB is an essential gene for placentation, it was conditionally deleted in the embryo proper. *JunB*$^{\Delta/\Delta}$ mice are born viable, but develop severe low turnover osteopenia caused by apparent cell-autonomous osteoblast and osteoclast defects before a chronic myeloid leukemia-like disease. Although JunB was reported to be a negative regulator of cell proliferation, *junB*$^{\Delta/\Delta}$ osteoclast precursors and osteoblasts show reduced proliferation along with a differentiation defect in vivo and in vitro. Mutant osteoblasts express elevated p16^{INK4a} levels, but exhibit decreased cyclin D1 and cyclin A expression. Runx2 is transiently increased during osteoblast differentiation in vitro, whereas mature osteoblast markers such as osteocalcin and bone sialoprotein are strongly reduced. To support a cell-autonomous function of JunB in osteoclasts, *junB* was inactivated specifically in the macrophage–osteoclast lineage. Mutant mice develop an osteopetrosis-like phenotype with increased bone mass and reduced numbers of osteoclasts. Thus, these data reveal a novel function of JunB as a positive regulator controlling primarily osteoblast as well as osteoclast activity.

Introduction

Bone is subject to constant remodelling as a result of the complementary activities of two main cell types. Osteoblasts (the bone-forming cells) originate from mesenchymal progenitors and osteoclasts (the bone-resorbing cells) derive from hematopoietic precursors within the monocyte–macrophage lineage (Karsenty and Wagner, 2002). Both of these cell types interact at the progenitor level through signals that influence activation and differentiation. Osteoblast progenitors or bone marrow stromal cells are stimulated by agents such as 1,25-dihydroxyvitamin D_3 or parathyroid hormone. After stimulation, osteoblasts synthesize macrophage colony–stimulating factor (M-CSF) and the tumor necrosis factor-related cytokine receptor activator of NFκB ligand (RANKL), two cytokines essential for osteoclastogenesis (Karsenty and Wagner, 2002). During osteoblast and osteoclast proliferation and differentiation, precursor cells express different stage-specific markers. The transcriptional mechanisms responsible for the expression of stage-specific genes are still not fully understood. However, some osteoclast-specific genes such as tartrate-resistant acid phosphatase (TRAP), carbonic anhydrase II, or matrix metalloproteinase-9 (MMP-9) and osteoblast marker genes such as osteocalcin or bone sialoprotein have been shown to be target genes of the transcription factor activator protein-1 (AP-1; Yamauchi et al., 1996; Aslam et al., 1999; David et al., 2001; Simon et al., 2001). The transcription factor NFATc1 has recently been identified as a key regulatory protein, which together with the AP-1 protein c-Fos, controls the terminal differentiation of osteoclasts downstream of RANKL signaling (Takayanagi et al., 2002).

AP-1 is a dimeric transcription factor composed of members of the Jun family (c-Jun, JunB, and JunD), which form homodimers or heterodimers with members of the Fos family

L. Kenner and A. Hoebertz contributed equally to this paper.

Address correspondence to Erwin F. Wagner, Research Institute of Molecular Pathology, Dr. Bohr-Gasse 7, A-1030 Vienna, Austria. Tel.: 43-1-797-30-888. Fax: 43-1-798-71-53. email: wagner@imp.univie.ac.at

Key words: AP-1; conditional gene targeting; osteoblasts; osteopenia; osteopetrosis

Abbreviations used in this paper: AP-1, activator protein-1; CML, chronic myeloid leukemia; ES, embryonic stem; M-CSF, macrophage colony–stimulating factor; MMP-9, matrix metalloproteinase-9; RANKL, receptor activator of NFκB ligand; TRAP, tartrate-resistant acid phosphatase.

(c-Fos, Fra-1, Fra-2, and FosB) and ATF proteins (ATF-2, ATF-3, ATFa, and ATF-4; Shaulian and Karin, 2002). AP-1 modulates the transcription of target genes by binding to their TRE or CRE consensus element (Shaulian and Karin, 2002). Although AP-1 is involved in different biological processes such as proliferation, differentiation, apoptosis, and transformation, specific roles for AP-1 in skeletal development have been uncovered mainly through genetic studies in mice (Jochum et al., 2001; Eferl and Wagner, 2003). The absence of c-Fos leads to a complete block in osteoclast differentiation and to the development of osteopetrosis (Grigoriadis et al., 1994). Conversely, transgenic mice overexpressing c-Fos develop osteosarcomas due to osteoblast transformation (Grigoriadis et al., 1993). Transgenic mice overexpressing Fra-1 or ΔFosB, a splice variant of FosB, develop osteosclerosis caused by accelerated differentiation of osteoprogenitors into mature osteoblasts (Jochum et al., 2000; Sabatakos et al., 2000). Moreover, the loss of Fra-1 results in an osteopenic phenotype due to reduced bone formation (unpublished data).

In contrast to Fos proteins, little is known about the role of Jun proteins in bone development. Inactivation of c-Jun and JunB in mice results in embryonic lethality (Eferl et al., 1999; Schorpp-Kistner et al., 1999), whereas mice lacking JunD are viable (Thepot et al., 2000). Overexpression of c-Jun (Grigoriadis et al., 1993), JunB (Schorpp et al., 1996), or JunD (unpublished data) did not result in an overt bone phenotype. However, chondrocyte-specific inactivation of c-Jun results in severe scoliosis caused by failure of intervertebral disc formation, suggesting that c-Jun is a regulator of sklerotomal differentiation (Behrens et al., 2003). In addition, c-Jun was found to be essential for efficient osteoclastogenesis in vitro (David et al., 2002). The embryonic lethality caused by lack of JunB and characterized by placental defects can be rescued by inter-crossing $junB^{+/-}$ with Ubi-*junB* transgenic mice. However, these mice develop a chronic myeloid leukemia (CML)-like disease due to loss of expression of the *junB* transgene in the myeloid lineage (Passegue et al., 2001), implying that JunB is a negative regulator of myeloid progenitors and can act as a tumor suppressor gene.

Here, we report that the embryonic lethality in the absence of JunB can also be rescued using a conditional gene-targeting approach. Mice with a floxed *junB* allele were generated and crossed to mice carrying the Mox2-Cre (MORE-*cre*) knock-in allele, which restricts Cre recombinase activity to the embryo (Tallquist and Soriano, 2000). Mutant mice with conditional deletion of *junB* in the embryo—$junB^{\Delta/\Delta}$ mice—are viable and born with Mendelian ratios. However, loss of JunB results in reduced bone formation and severe low turnover osteopenia besides the CML-like disease. The osteopenia is mainly due to a cell-autonomous osteoblast and osteoclast proliferation and differentiation defect, revealing a novel role for JunB as a positive regulator of cell proliferation in bone cells.

Results

Conditional rescue of the embryonic lethality

To investigate the role of JunB in advanced embryonic development and adulthood, a floxed allele of *junB* ($junB^{f/f}$) was introduced into embryonic stem (ES) cells by homologous recombination (Fig. 1 A). The neomycin resistance and the thymidine kinase genes were removed by flp-mediated recombination, and correct targeting was confirmed by Southern blot analysis. Homozygous $junB^{f/f}$ mice are viable and indistinguishable from wild-type mice, indicating that the floxed *junB* alleles are not causing an overt phenotype. To rescue the embryonic lethality likely caused by placental defects, $junB^{f/f}$ mice were crossed to MORE-Cre mice, where Cre recombinase is expressed from the epiblast-specific *Mox2* locus, thus restricted to the embryo proper (Tallquist and Soriano, 2000). MORE-Cre $junB^{f/f}$ ($junB^{\Delta/\Delta}$) mice are born with Mendelian frequencies. However, already at the age of 4 wk, mutant mice developed a severe osteopenia that progressed with increasing age (Fig. 1 B; Fig. 2, A and C). After 3–6 mo, mutant mice acquired a myeloproliferative CML-like disease with massive infiltration of neutrophilic granulocytes in bone marrow and spleen (Fig. 1 C), as has previously been described for mice lacking JunB in the myeloid compartment (Passegue et al., 2001). The efficiency of the *junB* deletion was confirmed in different tissues and in isolated bone cells of adult $junB^{\Delta/\Delta}$ mice by Southern blot analysis (Fig. 1 D). Moreover, the absence of *junB* expression was also verified by Northern blot using RNA from different tissues (Fig. 1 E) and by Western Blot for JunB protein from isolated osteoblasts and osteoclasts (Fig. 1 F).

Severe osteopenia in $junB^{\Delta/\Delta}$ mice

No obvious bone phenotype was observed in $junB^{\Delta/\Delta}$ newborns, whereas the number of osteoblasts was already reduced at 7 d of age (unpublished data). At 4 wk of age, the mice had thinner and brittle bones. At 6 mo of age, tibia bone length was reduced in $junB^{\Delta/\Delta}$ mice compared with controls (21 ± 1 mm in $junB^{f/\Delta}$ and 16 ± 1 mm in $junB^{\Delta/\Delta}$ mice). Detailed histological analysis of vertebrae revealed decreased bone mass at the age of 1 mo, which progressed rapidly until the age of 6 mo (Fig. 2 A). Cortical bone thickness, the most important parameter for biomechanical strength, was analyzed using micro-CT. Femoral cortical thickness was reduced from 350 μm in $junB^{f/\Delta}$ controls to 142 μm in $junB^{\Delta/\Delta}$ mice at 6 mo of age (Fig. 2 B). Biomechanical measurements (force to failure) using three-point bending revealed that femoral diaphyseal bone strength of $junB^{\Delta/\Delta}$ animals was significantly decreased (Fig. 2 F). When force to failure is corrected for geometry, the breaking strength of the bones in $JunB^{f/\Delta}$ is 114.63 MPa and in $JunB^{\Delta/\Delta}$ 79.05 MPa, demonstrating that the intrinsic property as well as the breaking load of the bones is JunB dependent.

Static histomorphometric analysis on lumbar vertebral bodies of $junB^{\Delta/\Delta}$ and control mice at three different time points (1, 3, and 6 mo) revealed that bone volume and trabecular thickness are up to 30–40% decreased in $junB^{\Delta/\Delta}$ mice (Fig. 2, C and D). However, the number and separation, i.e., the distance between trabeculae, were not significantly changed (Fig. 2 E; unpublished data). These results are characteristic for low turnover osteopenia, which results from a defect in osteoblast function. The number of osteoblasts was reduced by up to 90% (Fig. 2 G), and osteoclast numbers were also reduced by 70% (Fig. 2 H). Similar results were obtained for tibial metaphyses (unpublished data). Consistent with lower osteoclast numbers, bone resorption in vivo was also significantly reduced in 1- and 3-mo-old mice, as assessed by measuring urine deoxypyridinoline cross-links (Fig. 2 I).

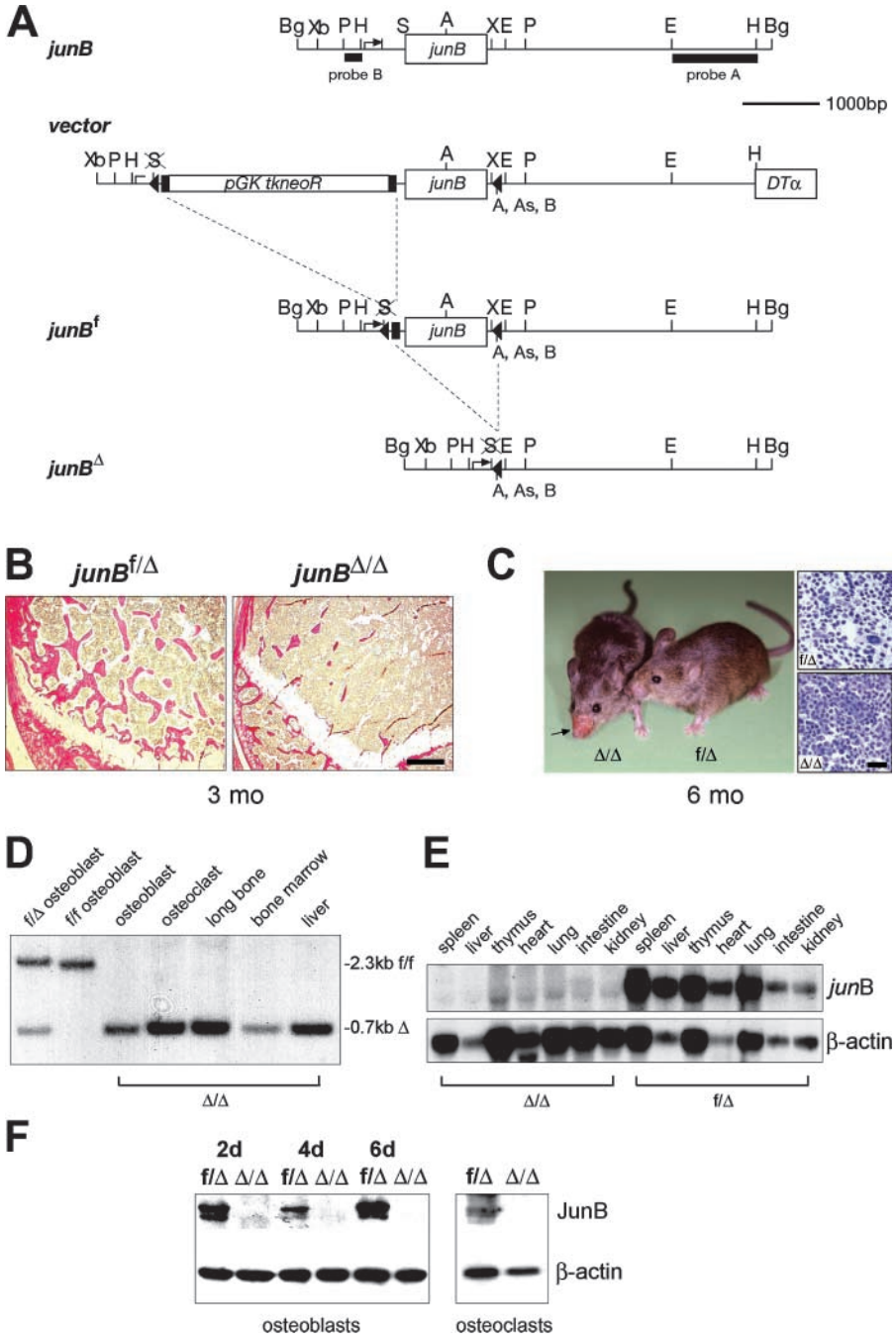

Figure 1. **Generation of mice harboring a floxed *junB* allele.** (A) Schematic representation of the targeting strategy used to generate a floxed allele of *junB*. The *junB* ORF is represented by a rectangle. The thymidine kinase-neomycin resistance gene (tkneoR) and the diphtheria toxin α (DTα) gene are indicated; *loxP* sites are shown as triangles. Bg, BglII; Xb, XbaI; X, XhoI; P, PstI; H, HindIII; S, SmaI; A, AccI; As, Asp780; B, BalI, E, EcoRI. A 3′ HindIII/EcoRI probe (probe A) was used for Southern analysis of BalI-digested genomic DNA to identify the targeted allele in the ES cells. To detect the deletion of the floxed allele, a 5′ PstI/HindIII probe (probe B) was used to analyze PstI-digested genomic DNA for Southern blot. *JunB* transcripts on Northern blots were detected using an EcoRI probe of *junB*. (B) Histological analysis of the metaphyseal regions (distal femur) of $junB^{f/\Delta}$ control and $junB^{\Delta/\Delta}$ mice at 3 mo of age (Giemsa). Bar, 250 μm. (C) A 6-mo-old $junB^{\Delta/\Delta}$ mouse and a $junB^{f/\Delta}$ control littermate are shown. Arrow indicates areas of CML-associated infiltrates. Histological sections (HE) of normal bone marrow in $junB^{f/\Delta}$ control (top right) and myeloproliferative infiltrates in $junB^{\Delta/\Delta}$ mice (bottom right). Bar, 20 μm. (D) Southern blot showing deletion of *junB* in osteoblasts, osteoclasts, long bone, bone marrow, and liver. (E) mRNA expression of *junB* in different tissues of 3-mo-old $junB^{\Delta/\Delta}$ mice and wild-type controls; β-actin serving as loading control. (F) Western blot showing protein expression levels of JunB in osteoblasts after 2, 4, and 6 d of proliferation, and in osteoclasts, both cultured in proliferative conditions.

Dynamic histomorphometric analysis showed that cortical bone formation rate was reduced to 60% after 1 mo and to 40% after 3 mo (Fig. 2 J), whereas trabecular bone formation rate was reduced to 70% after 1 mo and to 30% after 3 mo (Fig. 2 K). Osteocyte numbers and morphology within the tibial cortex were not changed, and polarized microscopy demonstrated that the cortex in $junB^{\Delta/\Delta}$ mice consisted of normal lamellar bone, as seen in controls (unpublished data). The structure of the epiphyseal growth plate and the cartilage seemed normal (unpublished data).

Because loss of JunB in the myeloid compartment in Ubi-*junB*/$junB^{-/-}$ mice has previously been shown to cause a CML-like disease (Passegue et al., 2001), we wanted to exclude that the development of CML is responsible for the bone phenotype in $junB^{\Delta/\Delta}$ mice. Histomorphometry of 11-mo-old Ubi-*junB*/$junB^{-/-}$ mice, where JunB expression is lost in the granulocyte compartment, was performed. No decrease in bone volume, bone formation rate, and cellular parameters could be detected in leukemic Ubi-*junB*/$junB^{-/-}$ mice compared with controls (unpublished data), proving that the described bone phenotype is independent of the CML-like disease.

Osteoblast defects in the absence of JunB

To investigate the cellular defects leading to osteopenia in $junB^{\Delta/\Delta}$ mice, osteoblast markers were first analyzed in vivo by in situ hybridization and real-time PCR of total femoral bone RNA of 6-mo-old $junB^{\Delta/\Delta}$ and control mice. The numbers of

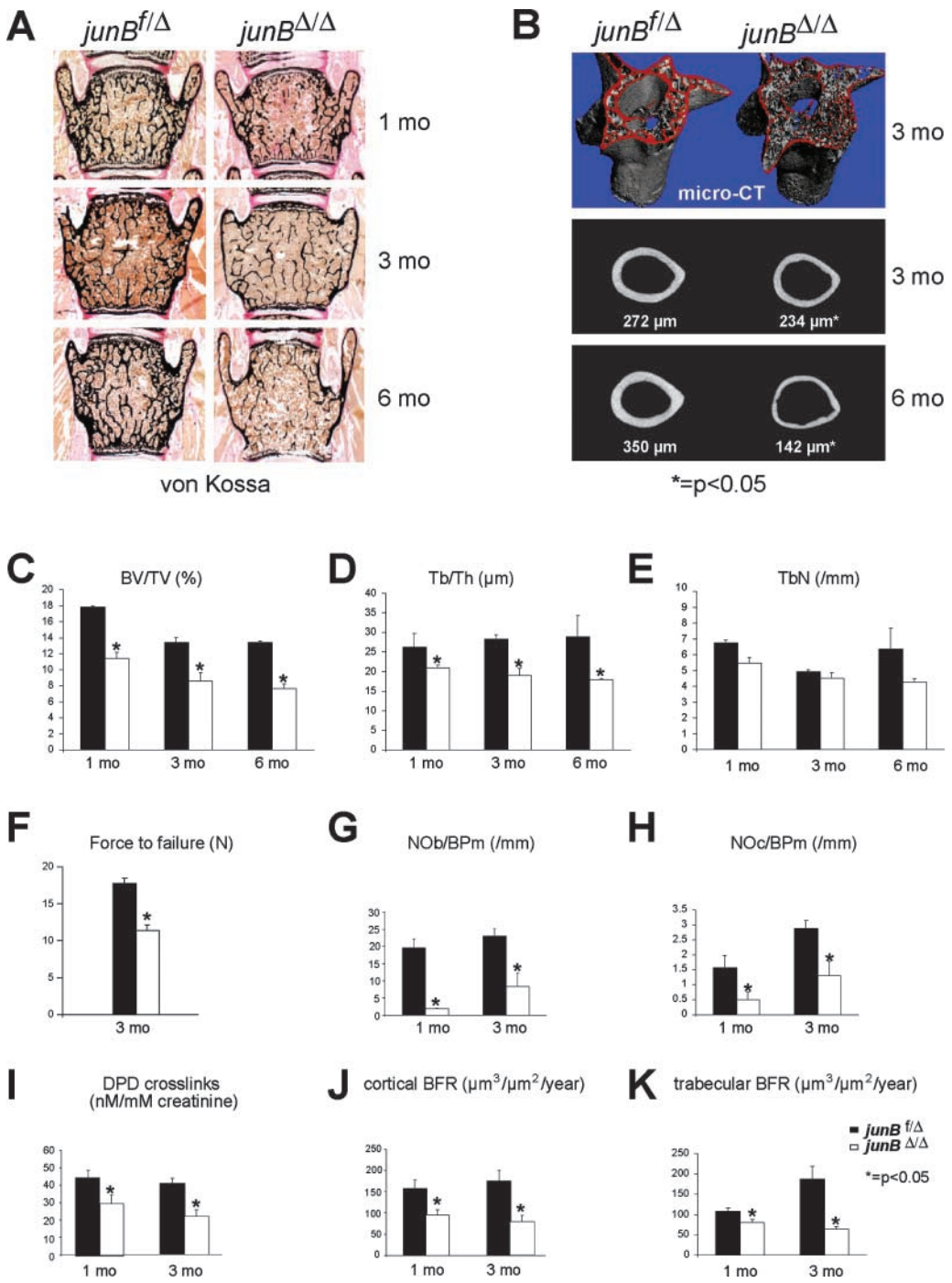

Figure 2. **Analysis of the bone phenotype of *junB*$^{\Delta/\Delta}$ mice.** (A) Histological analysis of vertebrae of *junB*$^{f/\Delta}$ control littermate and *junB*$^{\Delta/\Delta}$ mice at 1, 3, and 6 mo of age. Trabecular and cortical bone is stained black (von Kossa staining). (B) micro-CT of vertebral bodies of 3-mo-old *junB*$^{f/\Delta}$ control littermate and *junB*$^{\Delta/\Delta}$ mice. The surfaces of trabecular and cortical bone are shown in red. Cortical micro-CT of 3- and 6-mo-old femora from *junB*$^{f/\Delta}$ and *junB*$^{\Delta/\Delta}$ control mice. Histomorphometrical analysis of structural bone parameters in 1-, 3-, and 6-mo-old mice (C–E), and of cellular and dynamic parameters in 1- and 3-mo-old mice (G–K). (C) Trabecular bone volume (BV/TV; %). (D) Trabecular thickness (Tb/Th; mm). (E) Trabecular number (TbN; /mm). (F) Femoral whole-bone mechanical properties were determined by measuring fracture energy (force to failure; N). (G) Number of osteoblasts/bone perimeter (NOb/BPm; /mm). (H) Number of osteoclasts/bone perimeter (NOc/BPm; /mm). (I) Urine deoxypyridinoline cross-links (nM/mM creatinine) in 1- and 3-mo-old mice. (J) Cortical bone formation rate (mm^3/mm^2/year). (K) Trabecular bone formation rate (mm^3/mm^2/year). Bars represent mean values ± SD. Results from five mice of each genotype are shown.

junB$^{\Delta/\Delta}$ cells expressing *osteopontin*, an early osteoblast and late hypertrophic chondrocyte marker, were unchanged compared with controls. In contrast, both the numbers of cells expressing *collagen type 1a2* and *osteocalcin*, a late marker of osteoblast function, and the signal intensity per cell were severely reduced, supporting an osteoblast defect in vivo (Fig. 3 A). In total bone extracts, mRNA levels of *runx2* were significantly increased, whereas mRNA levels of *alkaline phosphatase* (*alp*), *bone sialoprotein* (*bsp*), *osteocalcin* (*oc*), *collagen type 1a2* (*col1a2*), *rankl*, and *osteoprotegerin* were significantly reduced,

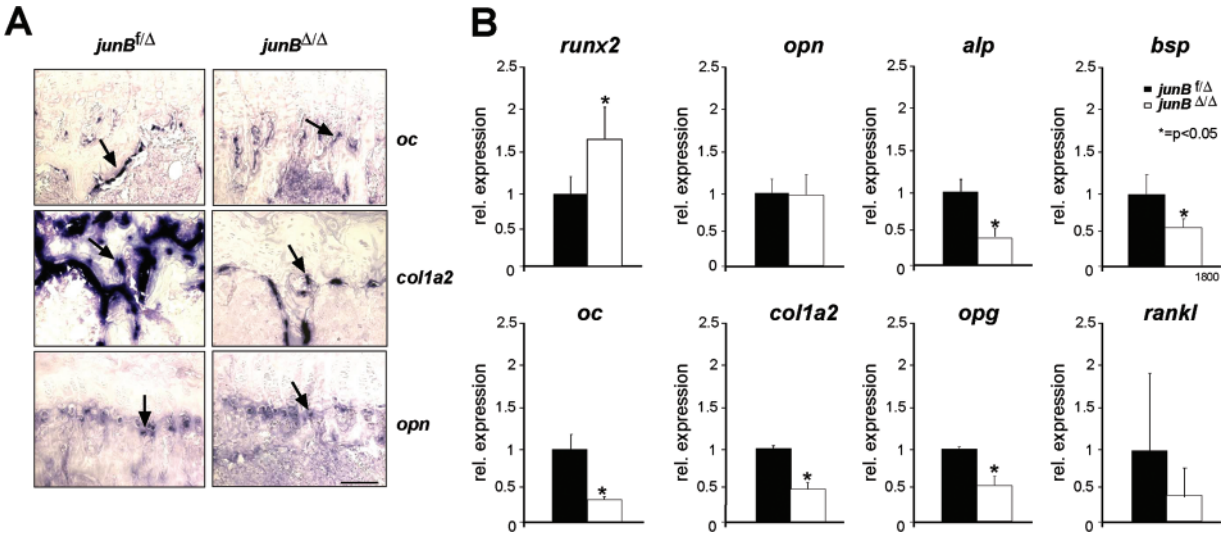

Figure 3. **Analysis of osteoblast marker gene expression in vivo.** (A) Analysis of *osteocalcin* (*oc*), *collagen type 1a2* (*col1a2*), and *osteopontin* (*opn*) by in situ hybridization. Shown are the distal metaphysis in 2-mo-old mice; osteoblasts indicated by arrows. Bar, 50 μm. (B) Real-time PCR of *runx2*, *osteopontin* (*opn*), *alkaline phosphatase* (*alp*), *bone sialoprotein* (*bsp*), *osteocalcin* (*oc*), *collagen1a2* (*col1a2*), *osteoprotegerin* (*opg*), and *rankl* from total femoral bone mRNA of 6-mo-old mice. Expression levels were normalized to tubulin expression. Values are presented as relative expression. Bars represent mean values ± SD ($n = 3$).

in agreement with lower absolute numbers of osteoblasts in vivo (Fig. 2 G). Expression levels of *osteopontin* (*opn*) were unchanged (Fig. 3 B). Because RANKL synthesis by osteoblasts is essential for efficient osteoclastogenesis, the decreased synthesis due to reduced osteoblast numbers could also contribute to reduced osteoclast numbers in vivo, in addition to a cell-autonomous osteoclast differentiation defect (see Fig. 5). Moreover, in vivo analysis of osteoblast proliferation revealed a 50% reduction of Ki-67–positive osteoblasts in long bones ($junB^{f/\Delta}$ 55.6 ± 3.1%; $junB^{\Delta/\Delta}$ 29.7 ± 1.1% Ki-67–positive osteoblasts).

Next, proliferation and differentiation of primary calvarial osteoblasts were analyzed in vitro. The proliferation rate of $junB^{\Delta/\Delta}$ calvarial osteoblasts, determined by BrdU incorporation, was reduced by 50% after a 2-d culture period (Fig. 4 A). To study the molecular mechanism responsible for the osteoblast proliferation defect, flow cytometry and Western Blot analyses of cell cycle regulators were performed. Serum-starved and restimulated $junB^{\Delta/\Delta}$ osteoblasts showed reduced BrdU incorporation by FACS® analysis and delayed S-phase entry (Fig. 4 B). Mutant osteoblasts expressed both reduced amounts of cyclin D1 and cyclin A protein, whereas the expression of cyclin E and p21 were not changed (Fig. 4 C, and unpublished data). Interestingly, the expression of $p16^{INK4a}$ was up-regulated in $junB^{\Delta/\Delta}$ osteoblasts (Fig. 4 C), contrasting previous results in fibroblasts and granulocytes (Passegue and Wagner, 2000; Passegue et al., 2001). Levels of c-Jun were increased at all time points (Fig. 4 C) confirming analysis from other cell types (Chiu et al., 1989).

The differentiation potential of mutant osteoblasts was analyzed in vitro by staining high density cultures after 3 wk for the deposition of mineralized ECM (bone nodules) and for alkaline phosphatase activity. In mutant cultures, bone nodule formation was severely reduced and alkaline phosphatase–positive cells were almost absent (Fig. 4 D). To study candidate molecules responsible for the observed cellular defects, the expression of marker genes was analyzed by real-time PCR in cultures at d 1, 5, 8, 12, and 16 during in vitro differentiation. Interestingly, expression levels of transcripts for *runx2* and *rankl* were transiently up-regulated at d 5 and 8 in $junB^{\Delta/\Delta}$ cells, whereas mRNA expression of *collagen type 1a2* (*col1a2*), *alkaline phosphatase* (*alp*), *bone sialoprotein* (*bsp*), and *osteocalcin* (*oc*) were strongly reduced at all time points in mutant osteoblasts (Fig. 4 E). mRNA expression of *osteopontin* and *osteonectin* were not changed (unpublished data). To determine whether the defect in osteoblast differentiation is not due to the reduced proliferative potential, we counted cell numbers after plating cells at high density normally used for differentiation experiments (5×10^5 cells/6-well). After 6 d in culture, control osteoblasts reached a density of 1.4×10^6 cells/well, whereas $junB^{\Delta/\Delta}$ osteoblasts had a slightly reduced cell density of 1.2×10^6 cells/well. Thus, mutant osteoblasts are capable of acquiring a multilayer structure necessary for differentiation, yet late osteoblast markers are down-regulated.

JunB affects osteoclast differentiation and proliferation

To study the role of JunB in osteoclast differentiation, bone marrow precursor cells were cultured for 6 d in the presence of M-CSF and RANKL (Fig. 5, A–C). When cultured on plastic, differentiation of $junB^{\Delta/\Delta}$ precursors into multinucleated, TRAP-positive osteoclasts was drastically reduced to 10% compared with control cultures (Fig. 5 B). This differentiation defect could not be fully rescued by culture on bovine bone slices (Fig. 5 C) or by reciprocal coculture experiments on $junB^{\Delta/\Delta}$ or wild-type osteoblast feeder layers (Fig. 5 D). However, mutant and wild-type osteoblasts had the same potential to support osteoclastogenesis of control bone marrow, indicating a cell-autonomous osteoclast differentiation defect in $junB^{\Delta/\Delta}$ mice. Osteoclast resorptive activity was evaluated by reflective light microscopy and was adjusted for the number of osteoclasts. There was no difference in relative resorptive activity, indicating that mutant osteoclasts are functional (Fig. 5 E).

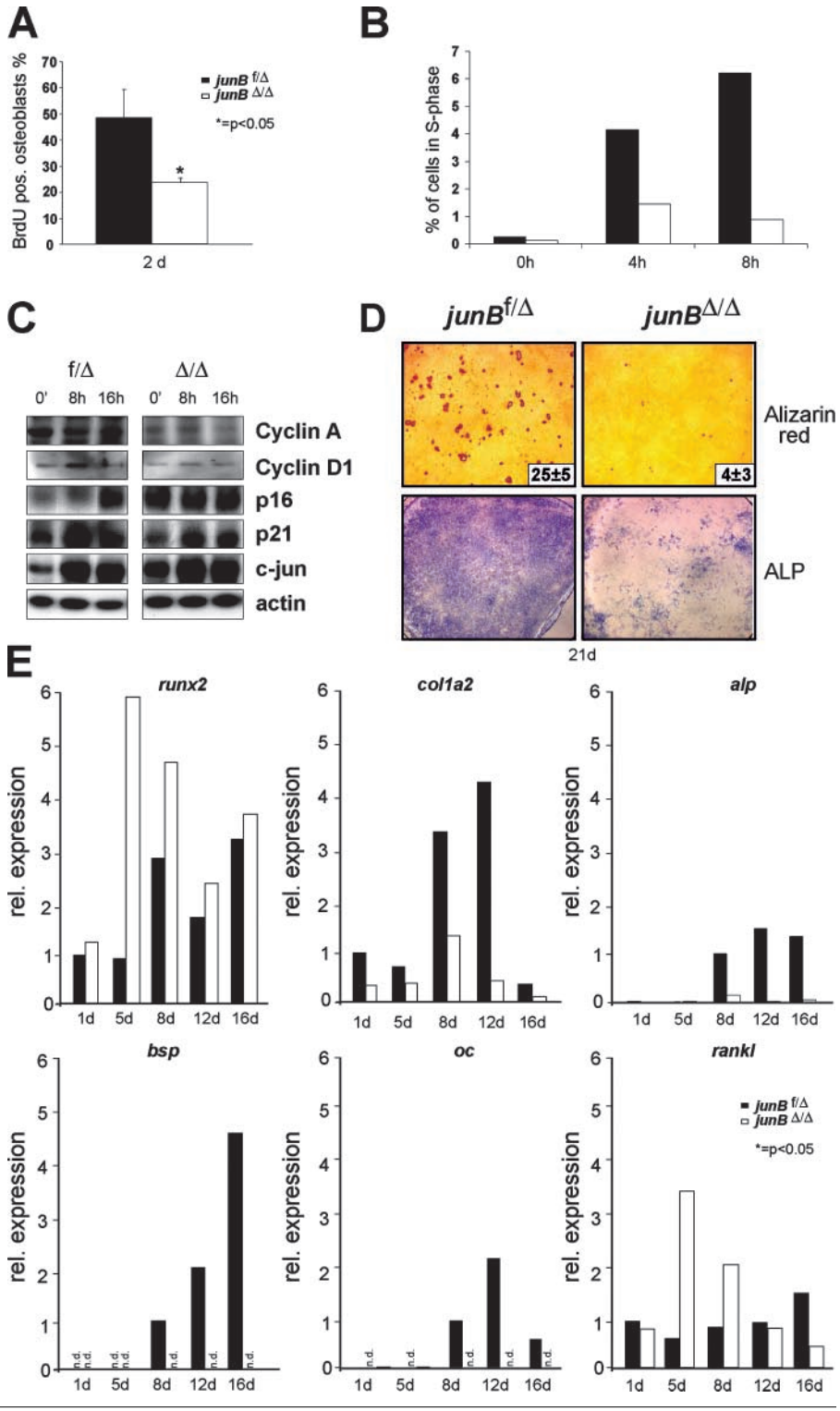

Figure 4. **Analysis of osteoblast proliferation and differentiation in vitro.** (A) BrdU incorporation into *junB*$^{f/\Delta}$ control and *junB*$^{\Delta/\Delta}$ osteoblast cultures and numbers of BrdU-positive osteoblasts. Bars represent mean values ± SD ($n = 3$). (B) FACS® analysis of BrdU incorporation in serum-starved and restimulated control and *junB*$^{\Delta/\Delta}$ osteoblasts. (C) Cell cycle profile in synchronized serum-induced osteoblasts of cyclin A, cyclin D1, p16, p21, c-Jun, and actin using Western blot analysis. (D) Formation of mineralized ECM by neonatal calvarial osteoblast cultures from *junB*$^{f/\Delta}$ and *junB*$^{\Delta/\Delta}$ control littermates. Mineralized nodules are stained by Alizarin S red (top). Osteoblast cultures were also stained for alkaline phosphatase activity (ALP, bottom). (E) Real-time PCR of *runx2*, *collagen type 1a2* (*col1a2*), *alkaline phosphatase* (*alp*), *bone sialoprotein* (*bsp*), *osteocalcin* (*oc*), and *rankl* from *junB*$^{f/\Delta}$ control and *junB*$^{\Delta/\Delta}$ osteoblasts at 1, 5, 8, 12, and 16 d of differentiation. Expression levels were normalized to tubulin expression and were presented as relative expression. One representative result of three independent osteoblast cultures is shown.

Proliferation of osteoclast precursors was measured by BrdU incorporation of preosteoclasts cultured on plastic only in the presence of M-CSF. A 50% reduction in incorporation was observed in mutant cultures after a 2-d culture period (Fig. 5 F), whereas no apparent difference in TUNEL-positive osteoclasts was detected (unpublished data). These data demonstrate that JunB is necessary for both proliferation of osteoclast progenitors as well as for osteoclast differentiation in vitro.

To study gene expression in the osteoclast lineage, real-time PCR was performed on primary differentiated osteoclasts and from total bone RNA. The expression of mature osteoclast markers and known AP-1 target genes such as *TRAP*, *carbonic anhydrase II*, and *MMP-9* was significantly reduced in mutant osteoclasts in vitro (unpublished data) and in vivo (Fig. 5 G). Comparable levels were found for *cathepsin K* and *Microphthalmia-associated transcription factor* (Fig. 5 G; unpublished data), indicating that not all mature osteoclast markers

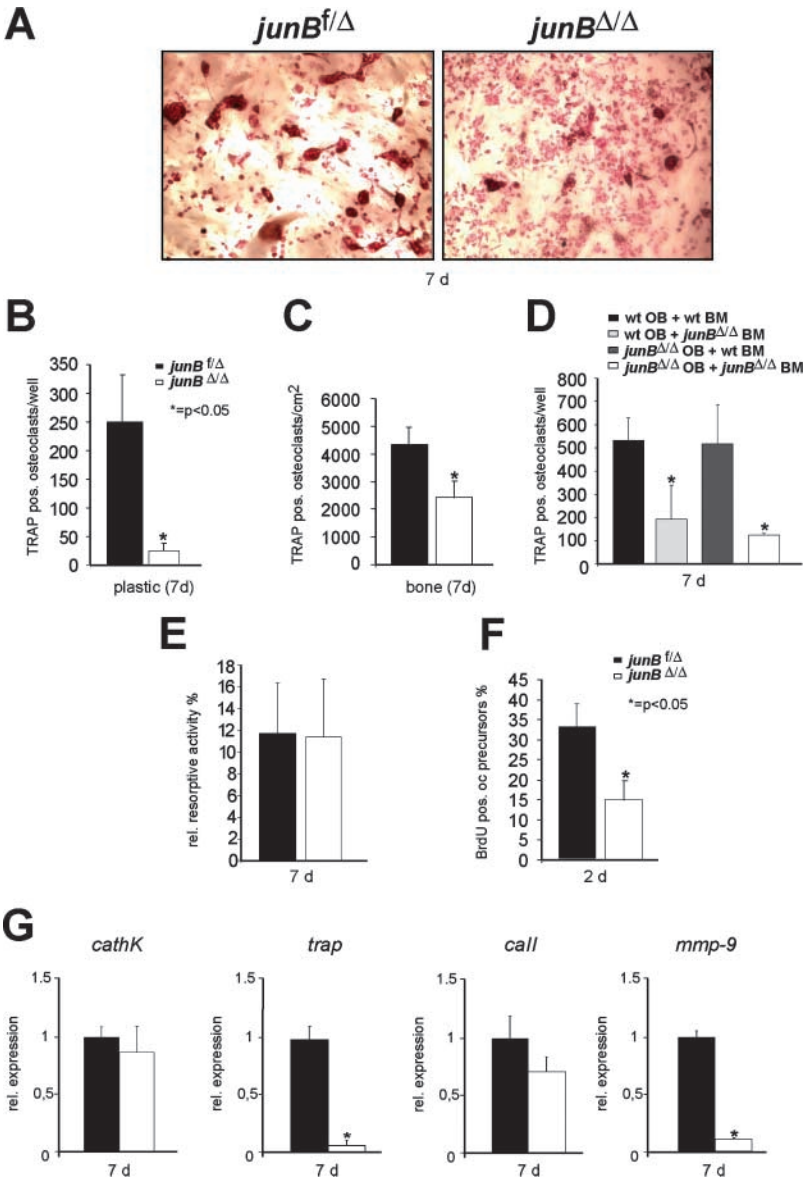

Figure 5. **Analysis of *junB*$^{\Delta/\Delta}$ osteoclast proliferation and differentiation in vitro.** (A) TRAP staining of osteoclasts cultured for 7 d on bovine bone discs induced by M-CSF and RANKL. (B) Numbers of differentiated osteoclasts grown on plastic for 7 d ($n = 4$). (C) Numbers of differentiated osteoclasts grown on bone for 7 d ($n = 4$). (D) Reciprocal cocultures of primary osteoblasts and bone marrow of the indicated genotypes under osteoclastogenic conditions followed by TRAP staining ($n = 4$). (E) Relative resorptive activity of *junB*$^{f/\Delta}$ control and *junB*$^{\Delta/\Delta}$ osteoclasts cultured on bovine bone for 7 d. Resorbed area was assessed by reflective light microscopy and corrected for the number of osteoclasts per disc. (F) BrdU incorporation into M-CSF–treated osteoclast precursors and numbers of BrdU-positive precursors after 2 d of culture ($n = 3$). (G) Real-time PCR analysis of *cathepsin K (cathK)*, *TRAP*, *carbonic anhydrase II* (*caII*), and *MMP-9* in *junB*$^{f/\Delta}$ and *junB*$^{\Delta/\Delta}$ femoral bone mRNA of 6-mo-old mice. Expression levels were normalized to tubulin expression. Values are presented as relative expression. Bars represent mean values ± SD ($n = 3$).

are down-regulated in the absence of JunB. Moreover, no changes in expression levels for *RANK*, *M-CSF receptor, GM-CSF receptor* α, and *G-CSF receptor* were found (unpublished data), suggesting that cytokine responsiveness of mutant osteoclast precursors is apparently not altered.

A cell-autonomous role of JunB in the osteoclast lineage

To test whether the osteoclast differentiation defect is intrinsic to the osteoclast lineage, *junB*$^{f/f}$ mice were crossed to Lysozyme-M-*cre* mice (Clausen et al., 1999), deleting *junB* in the macrophage–osteoclast lineage (*junB*$^{\Delta/\Delta m\phi/OC}$). Mice are born viable and without obvious signs of disease. Southern blot analysis showed complete deletion of *junB* in *junB*$^{\Delta/\Delta m\phi/OC}$ osteoclasts, whereas *junB* was only partially deleted in sorted granulocytes (unpublished data). Histological and radiographical analysis of long bones from 3-mo-old mutant mice showed increased trabecular bone volume and increased radiodensity, respectively (Fig. 6 A). In 11-mo-old mice, analysis of *junB*$^{\Delta/\Delta m\phi/OC}$ humeri revealed a profound increase in both numbers and diameter of trabeculae. The patterning of trabecular bone seemed to be irregular and occupied the whole diaphysis shaft (Fig. 6 B). Osteoclasts appeared frequently mononuclear and smaller than controls, indicating an osteoclast differentiation defect (Fig. 6 C). The number of TRAP-positive osteoclasts in vivo was greatly reduced, and histomorphometric analysis revealed a 50% reduction in osteoclast numbers (Fig. 6 D).

Differentiation of *junB*$^{\Delta/\Delta m\phi/OC}$ bone marrow precursors into osteoclasts in vitro was significantly reduced to 16% of control osteoclasts on both plastic (unpublished data) and bone surfaces (Fig. 6 E). Moreover, proliferation of mutant osteoclast precursors, as measured by BrdU incorporation of M-CSF–treated preosteoclasts, was slightly, but not significantly, reduced. These data indicate that loss of *junB* in osteoclast precursors results mainly in a cell-autonomous reduction of osteoclast differentiation in vivo and in vitro.

Discussion

Because JunB is essential for mouse development, a conditional gene-targeting approach was used to study its function

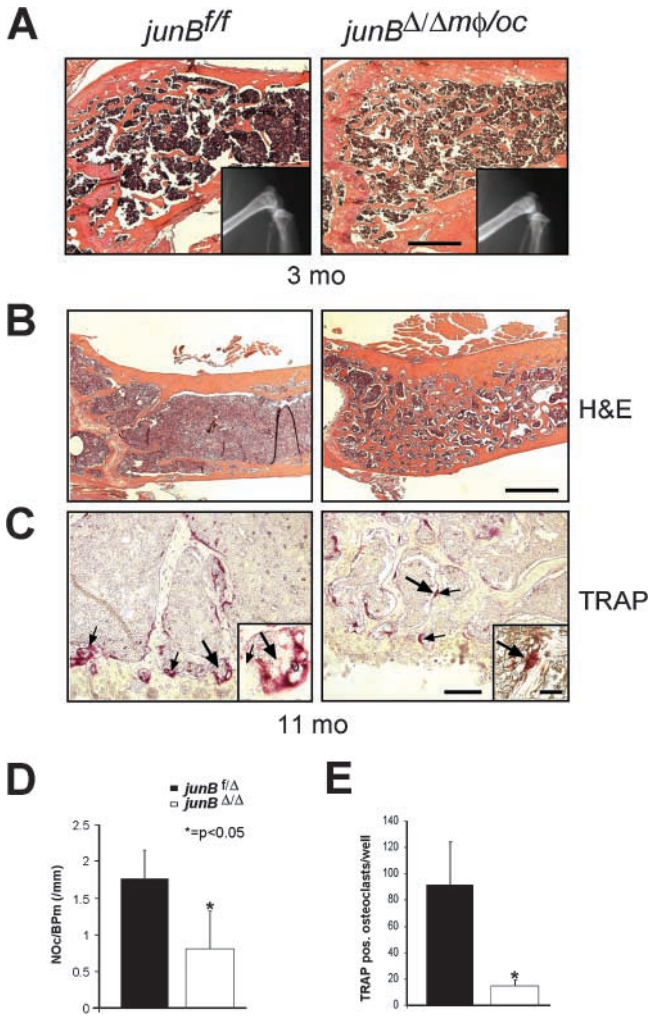

Figure 6. **Characterization of *junB*$^{\Delta/\Delta m\phi/OC}$ Lysozyme-M-Cre mice.** (A) Histological analysis of the metaphyseal regions (proximal tibia) of wild-type and *junB*$^{\Delta/\Delta m\phi/OC}$ mice at 3 mo of age. Trabecular bone mass stained pink (HE staining). Bar, 500 μm. X-ray analysis of long bones of *junB*$^{f/f}$ control and *junB*$^{\Delta/\Delta m\phi/OC}$ mice at 3 mo of age (insets). (B) Histological analysis of the metaphyseal regions (distal humerus) of wild-type and *junB*$^{\Delta/\Delta m\phi/OC}$ mice at 11 mo of age. Bar, 500 μm. (C) TRAP staining of the distal metaphysis humeri (bar, 50 μm). Osteoclasts are stained red and indicated by arrows. Insets show osteoclasts at higher magnification (bar, 15 μm). (D) Numbers of osteoclasts/bone perimeter (NOc/BPm) in metaphyseal regions of 11-mo-old mice. (E) Numbers of differentiated TRAP-positive osteoclasts grown on bone (n = 4). Bars represent mean values ± SD.

postnatally. Embryonic lethality due to placental defects was rescued by the expression of *junB* in the parietal endoderm and trophectoderm lineage. This demonstrates that the described trophoblast defect is the cause of lethality, further supporting earlier findings with *junB*$^{-/-}$ES cells and tetraploid blastocyst injections (Schorpp-Kistner et al., 1999). The rescued *junB*$^{\Delta/\Delta}$ mice developed severe osteopenia as early as 1 mo after birth and exhibited decreased numbers of osteoblasts and osteoclasts in vivo. Bone formation, a function specific to the osteoblast and quantified by dynamic histomorphometry, and bone resorption, a function specific to the osteoclast and quantified by biochemical analysis of crosslink excretion, were both decreased in *junB*$^{\Delta/\Delta}$ mice compared with controls. Because *junB*$^{\Delta/\Delta}$ mice are osteopenic, the reduction in bone formation exceeds the decrease in bone resorption, which by itself would lead to more bone.

Reduced osteoclast differentiation in vivo might also be partly due to reduced numbers of osteoblasts, and consequently, reduced RANKL production in vivo. Moreover, the defects in mice lacking *junB* were cell autonomous as revealed by ex vivo cultures. Because the trabecular microarchitecture remained unchanged, this phenotype resembles severe low turnover osteopenia, similar to senile osteoporosis in aged humans. As previously described for mice lacking *junB* in the myeloid compartment (Passegue et al., 2001), mutant mice also acquire a myeloproliferative CML-like disease after 3–6 mo.

A function of JunB as a transcriptional regulator important for both osteoblast and osteoclast proliferation and differentiation has not yet been documented in vivo using mice lacking JunB. Previous in vitro experiments had suggested a role for JunB in inducing the differentiation of mesenchymal progenitors toward the osteoblastic phenotype, and *junB* mRNA transcripts have been shown to be present during the proliferative period and during late stages of osteoblast development (McCabe et al., 1995). In synchronized and proliferating osteoblasts lacking *junB,* we observed a delay in S-phase entry, reduced levels of cyclin D1 and cyclin A protein, and increased levels of the CDK inhibitor p16^{INK4a}, suggesting that JunB positively regulates osteoblast proliferation. The finding that p16 is induced in the absence of JunB is particularly surprising because JunB has been found to be a negative regulator of cell proliferation by activating p16. In fibroblasts, JunB suppresses cell proliferation and induces premature senescence by transcriptional activation of p16 (Passegue and Wagner, 2000). Moreover, absence of JunB leads to myeloid leukemia with increased myeloid proliferation and decreased apoptosis caused by down-regulation of p16 expression and up-regulation of Bcl2 and of Bclx, clearly demonstrating that JunB can act as a tumor suppressor gene in mice (Passegue et al., 2001).

Furthermore, reduced cyclin D1 protein levels in proliferating *junB*$^{\Delta/\Delta}$ osteoblasts are also in contrast with previous analyses in fibroblasts. JunB was able to negatively regulate the cyclin D1 promoter at the transcriptional level (Bakiri et al., 2000), but also at the post-transcriptional level (Passegue et al., 2002). In contrast to JunB, c-Jun can transcriptionally activate cyclin D1 in fibroblasts (Wisdom et al., 1999). Consistent with the notion that JunB acts as a transcriptional repressor of c-Jun, *junB*$^{\Delta/\Delta}$ osteoblasts displayed higher levels of c-Jun protein. However, the increased c-Jun protein did not result in increased proliferation of osteoblasts. Decreased protein levels of cyclin A in mutant osteoblasts may additionally contribute to the reduced proliferation rate, confirming recent findings that JunB can also have a cell cycle–promoting role by transcriptionally activating the cyclin A promoter in fibroblasts (Andrecht et al., 2002). Because there is no apparent change in apoptosis in *junB*$^{\Delta/\Delta}$ osteoblasts, JunB does not appear to be necessary for the regulation of survival in osteoblasts. These data clearly indicate that JunB can act as a positive regulator of cell proliferation. Similar alterations in cyclin A and p16 expression, associated with defects in osteoblast proliferation in vitro, were observed in JunB-compromised cells isolated from Ubi-*junB*/*junB*$^{-/-}$ rescued mice (Hess et al., 2003).

Gene expression analyses of osteoblast-specific markers at different time points during osteoblast differentiation in

vitro showed that the mRNA expression levels of *collagen type 1a2*, *alkaline phosphatase*, *osteocalcin*, and *bone sialoprotein*, which are restricted to more mature osteoblasts, were strongly reduced in $junB^{\Delta/\Delta}$ osteoblasts, whereas *osteonectin* and *osteopontin* expression were not changed. Interestingly, RANKL expression was increased in mutant osteoblasts at early time points of culture, which might correlate with the fact that $JunB^{\Delta/\Delta}$ osteoblasts differentiate less and that immature osteoblasts have higher levels of RANKL expression.

Although *junB*-deficient osteoblasts have a severe proliferation defect, cells plated at high density are still capable of acquiring a multilayer structure. It cannot be excluded that the severe differentiation defect observed in mutant osteoblasts is partly caused by the reduced proliferative potential. However, both alkaline phosphatase and bone sialoprotein have been shown to be expressed in proliferating, osteocalcin-negative osteoblastic cells, whereas osteocalcin expression is only initiated after cells exit from log-phase growth (Malaval et al., 1999). Expression levels of all these genes are dramatically reduced in *junB*-deficient osteoblast cultures, suggesting a defect in osteoblast maturation in addition to the severe effect on proliferation.

Surprisingly, a progressive decrease in *osteocalcin* levels after a peak of expression at d 12 of culture was observed in wild-type cultures. This contrasts with the common knowledge of osteocalcin being a late marker of mature osteoblasts, and might be due to the heterogeneity of primary osteoblast cultures. Interestingly, *runx2* mRNA expression remains consistently up-regulated in the absence of JunB. Runx2 is an essential transcription factor for osteoblast differentiation and bone formation (Ducy et al., 1997; Komori et al., 1997). However, mice overexpressing Runx2 from the collagen type I promoter develop osteopenia due to an osteoblast maturation defect (Liu et al., 2001). Overexpression of a dominant-negative Runx2 at a late stage of osteoblast differentiation caused reduced expression of bone matrix, again resulting in osteopenia (Ducy et al., 1999). Therefore, Runx2 expression has to be tightly controlled, and the increased expression of *runx2* observed in $junB^{\Delta/\Delta}$ osteoblasts might be responsible for the defect in osteoblast maturation. This might indicate that JunB can function as a repressor of Runx2 at specific stages of osteoblast differentiation. However, transcriptional targets of Runx2 such as *collagen type I*, *osteocalcin*, and *alkaline phosphatase* are down-regulated in $junB^{\Delta/\Delta}$ osteoblasts in vivo and in vitro. Thus, JunB might also be involved in the induction of coactivators that are required for Runx2-dependent transcriptional activation.

To investigate the role of JunB in osteoclast differentiation, a number of putative AP-1 target genes as well as markers of the osteoclast lineage were analyzed in vitro and in vivo. Interestingly, $junB^{\Delta/\Delta}$ osteoclasts had a proliferation and differentiation defect, again contrasting the function of JunB as a negative regulator of cell proliferation. The loss of JunB expression does not influence either the expression of *Microphthalmia-associated transcription factor* or of *cathepsin K*. On the other hand, *TRAP*, *carbonic anhydrase II*, and *MMP-9* were down-regulated, all known AP-1 target genes and important for osteoclast function and recruitment (Schorpp-Kistner et al., 1999; David et al., 2001; Takayanagi et al., 2002).

To investigate whether the absence of JunB in the hematopoietic lineage would lead to a cell-autonomous bone phenotype, JunB was inactivated selectively in the macrophage–osteoclast lineage (Clausen et al., 1999). Interestingly, the mutant mice developed a severe osteopetrosis-like phenotype with markedly increased bone mass, strongly supporting the hypothesis of a cell-autonomous osteoclast defect. A similar but more severe osteopetrotic phenotype caused by a complete block in osteoclast differentiation is present in mice lacking c-Fos (Grigoriadis et al., 1994). Interestingly, this differentiation block could be rescued most efficiently by Fra-1 in vitro, but not by any of the Jun proteins (Matsuo et al., 2000). Therefore, it is possible that JunB might be the partner of c-Fos in osteoclastogenesis.

Together, mice lacking JunB only in the macrophage–osteoclast lineage are osteopetrotic and show increased bone mass, whereas they are severely osteopenic with a dominant osteoblast phenotype when JunB is missing in all bone cells. This implies that JunB is a key regulator of skeletogenesis affecting bone formation more strongly than bone resorption. These data further question the concept that there is a tight cross-talk between osteoblasts and osteoclasts during bone remodeling, which is in agreement with previous reports challenging this hypothesis (Corrall et al., 1998; Amling et al., 2000). The novel function of JunB as a positive regulator of bone remodelling opens new strategies to be used for preventing bone loss. Furthermore, $JunB^{\Delta/\Delta}$ mice provide an excellent model to study mechanisms leading to age-related bone loss.

Materials and methods

Generation of $junB^{f/f}$ mice

A floxed and frt-flanked neomycin resistance and thymidine kinase gene selection cassette was inserted into a SmaI site present in the 5′ untranslated region of *junB*. The 3′ loxP site was inserted into the XhoI site, 161 bp downstream of the translation stop codon. A diphtheria toxin gene was included for selection against random integrants. The linearized targeting construct was electroporated into HM-1 ES cells, and the identification of homologous recombinants by PCR using two sets of primers was performed as described previously (Schorpp-Kistner et al., 1999). The neomycin and thymidine kinase genes were deleted by transient transfection of a vector expressing flp recombinase. Two ES cell clones carrying a floxed allele of *junB* were injected into C57BL/6 blastocysts, and several chimeras from one ES cell clone transmitted the mutant allele to their offspring.

Mice

Mice carrying the floxed *junB* allele ($junB^{f/f}$) were crossed to MORE-Cre mice (Tallquist and Soriano, 2000) and to Lysozyme-M-Cre mice (Clausen et al., 1999; provided by I. Förster, University of Cologne, Cologne, Germany). The genetic background of this intercross was C57Bl/6 × 129. Mutant mice were intercrossed at least five times before bone histomorphometry to increase genetic homogeneity. Only female mice were used for quantitative histomorphometric measurements. Ubi-$junB/junB^{-/-}$ mice have been described previously (Passegue et al., 2001).

Southern, Northern, and Western blot analysis

For Southern blots, 10 μg genomic DNA was digested with PstI, yielding a 2.3-kb fragment for the floxed *junB* allele and a 0.7-kb fragment for the deleted *junB* allele. For detection of the bands, a 176-bp PstI/HindIII fragment of *junB* was used as a probe. Northern blot analysis was performed according to standard procedures using an EcoRI fragment of *junB* and a fragment of *β-actin* for loading control. Western blot analysis was performed according to standard procedures using anti-cyclin A, anti-p16, anti-p21, anti-cyclin D1, anti-cyclin E, anti-c-Jun (all from Santa Cruz Biotechnology, Inc.), anti-actin (Sigma-Aldrich), and anti-JunB (M. Yaniv, Institut Pasteur, Paris, France) antibodies.

In situ hybridization analysis

For nonradioactive in situ hybridization, bones from 3-mo-old mice were fixed overnight with neutral buffered 4% PFA at 4°C, decalcified for 10 d in

0.5 M EDTA, and embedded in paraffin. For in situ hybridization analysis, sections were deparaffinized and hybridization was performed according to standard procedures (Murtaugh et al., 1999). *Osteopontin, collagen type 1a2, and osteocalcin* mRNA were detected with DIG-labeled antisense probes (probes were provided by C. Hartmann, IMP, Vienna, Austria).

All sections from histological and in situ hybridization stainings were examined using a microscope (Axioskop2 mot; Carl Zeiss MicroImaging, Inc.) with Plan-Apochromat 20×/0.75 lenses, 40×/0.95 Korr lenses, and Plan-Neofluar 63×/1.25 oil lenses. Images were captured using a digital image capture camera (AxioCam *M*r Color; Carl Zeiss MicroImaging, Inc.). Image analysis was performed using tools provided in the AxioVision 3.1 software package (Carl Zeiss MicroImaging, Inc.). The images were further processed using Adobe Photoshop® 7.0.

X-ray analysis, histomorphometry, and histological analysis

Mice were killed at 1 and 7 d and at 4, 12, and 24 wk of age. After whole-animal contact radiography (using an x-ray cabinet; Faxitron), mice were killed by cervical dislocation and bones were fixed in 3.7% PBS-buffered formaldehyde. After dehydration, the undecalcified tibiae and lumbar spines were embedded in methylmethacrylate, and 5-μm sections were cut in sagittal plane on a rotation microtome (Cut 4060E; MicroTech) as described previously (Amling et al., 1999). Sections were stained with toluidine blue, and with modified von Kossa/van Gieson. Quantitative histomorphometry was performed on toluidine blue–stained, undecalcified proximal tibia and lumbar vertebra sections. For comparative histomorphometry, samples from five $JunB^{f/\Delta}$ and five $JunB^{\Delta/\Delta}$ mice at 1, 3, and 6 mo of age were used. Analysis of bone volume (percentage), trabecular thickness (micrometers), trabecular number (per mm), trabecular separation (micrometers), osteoblast number per bone perimeter (per mm), osteoclast number per bone perimeter (per mm), cortical thickness (micrometers), and trabecular and cortical bone formation rate ($\mu m^3/\mu m^2$/year) was performed according to standardized protocols of the American Society for Bone and Mineral Research (Parfitt et al., 1987) using the Osteomeasure histomorphometry system (Osteometrix). Experiments were performed in a blinded fashion. For assessment of dynamic histomorphometric indexes, mice were injected with calcein according to a standard double-labeling protocol (Amling et al., 1999). Fluorochrome measurements were made on two nonconsecutive 12-μm-thick sections per animal. Sections were mounted unstained in Fluoromount (Electron Microscopy Sciences).

Immunohistochemical staining for Ki67 (1:1,000, NCL-Ki67p; Novacostra) was performed on paraffin sections of formaldehyde-fixed, decalcified long bones using the ABC staining kit (Vector Laboratories) according to the manufacturer's recommendations.

Biomechanical testing and microcomputed tomography analysis (μCT)

Both femurs were stored in 50% ethanol-saline, transferred to isotonic saline, and stored at 4°C for 12 h before testing. A three-point bending was performed as described previously (Amling et al., 1999), using a commercial high precision instrument (Z2.5/TN 1S testing machine; Zwick GmbH & Co.). In brief, the ends of the bone were supported on two fulcra separated by 5 mm. With the posterior aspect of the femur resting on the fulcra, a load was applied from above to the anterior midshaft midway between the two fulcra, at a constant speed of 10 mm/min to failure. A chart recorder was used to generate a force-deformation curve. The stiffness was assessed as the slope of the force-deformation curve through its linear region. Experiments were performed in a blind fashion.

For three-dimensional histomorphometry and visualization of the vertebral bone structure, lumbar vertebra L6 of 3-mo-old mice was scanned in a microCT40 scanner (Scanco Medical) at a 6-μm resolution. The raw data were manually segmented and analyzed with μCT Evaluation Program v4.4A (Scanco Medical). For visualization, the segmented data were imported and displayed in μCT Ray v3.0 (Scanco Medical). For assessment of the femoral cortical thickness, femora were dissected out of 3- and 6-mo-old mice, and 20 planes were scanned at the midshaft in a microCT40 scanner at a 6-μm resolution. Cortical thickness was measured with the Distance 3D tool of the μCT Evaluation Program v4.4A (Scanco Medical). For all histomorphometrical analyses, the results from five mice of each genotype are shown.

Biochemical assays

We collected urine samples from sex- and age-matched mice. The urinary excretion of deoxypyridinoline cross-links was determined using the Pyrilinks-D ELISA and was expressed relative to urinary creatinine concentration (Metra Biosystems, Inc.).

PCR and real-time PCR analysis

PCR for genotyping of *junB*-deficient mice was performed with primers B1 5′-atcctgctgggagcggggaactgagggaag-3′, B2 5′-gggaactgagggaagccacgccgagaaagc-3′, B6 5′-agagtcgtcgtgatagaaaggc-3′, and B10 5′-aaacatacaaaatacgctgg-3′. Real-time PCR was performed with cDNA synthesized from 2 μg RNA with random primers using the ready-to-go™ cDNA kit (Amersham Biosciences) according to the manufacturer's protocols. RNA was isolated using the TRIzol® procedure (Sigma-Aldrich). For real-time PCR, cDNA was diluted to a final concentration of 3 ng/μl. For PCR reactions, light cycler Fast Start DNA Master SYBR® Green (Roche) was used. Three independent measurements per sample were performed. Primer pairs for osteoblast and osteoclast genes were used as follows: tubulin (391 bp) up 5′-caacgtcaagacggccgtgtg-3′, down 5′-gacagaggcaaactgagcacc-3′; runx2 (419 bp) up 5′-aacccacggccctccctgaactct-3′, down 5′-actggcggggtgtaggtaaaggtg-3′; col1a2 (445 bp) up 5′-tcgggcctgctggtgttcgtg-3′, down 5′-tgggcgcggctgtatgagttcttc-3′; ALP (479 bp) up 5′-cacgcgatgcaacaccactcagg-3′, down 5′-gcatgtccccgggctcaaaga-3′; OC (240 bp) up 5′-accctggctgcgctctgtctct-3′, down 5′-gatgcgtttgtaggcggtcttca-3′; BSP (432 bp) up 5′-taccggccacgctactttctttat-3′, down 5′-gaccgccagctcgttttcatcc-3′; osteonectin (417 bp) up 5′-acaacccctgccagaaccatcatt-3′, down 5′-cctccaggcgcttctcattctca-3′; osteopontin (425 bp) up 5′-ctccttgcgccacagaatg-3′, down 5′-tgggcaacagggatgaca-3′; MMP-9 (423 bp) up 5′-gccctacagcgccccctact-3′, down 5′-agacacgccccttgctgaaca-3′; cathepsin K (408 bp) up 5′-agggccaactcaagaagaaaact-3′, down 5′-tgccatagcccaccaccaacact-3′; TRAP (405 bp) up 5′-ggccggccactaccccatct-3′, down 5′-caccgtagcgacaagcaggactct-3′; carbonic anhydrase II (534 bp) up 5′-tgtcaacaacggccactcctt-3′, down 5′-tcagcatccccctcctcattg-3′; RANKL (407 bp) up 5′-gcttcactgcccagtctcatcgtt-3′, down 5′-gggccggtccgtgtactcatcct-3′; OPG (519bp) up 5′-ggaaccccagagcgaaacacagt-3′, down 5′-cttcttcccaggcaggctctccat-3′.

The comparative CT method was used to calculate the expression levels of RNA transcripts. The quantified individual RNA expression levels were normalized for the respective tubulin expression levels. Because we measured the relative RNA expression levels, the wild-type expression level was set as 1.

Osteoblast and osteoclast cultures

Primary osteoblasts were isolated from calvariae of neonatal (2–4-d-old) mice as described previously (Jochum et al., 2000). Cells were replated for differentiation at 5×10^5 cells/well, or for proliferation at 10^5 cells/well in a 6-well plate. For differentiation, medium was supplemented with 5 mM β-glycerophosphate and 100 μg/ml ascorbic acid. After 3 wk of culture, bone nodules were identified morphologically by Alizarin S red staining (Sigma-Aldrich). Staining of cultures for alkaline phosphatase activity was performed using a Sigma Kit 86R.

For differentiating and proliferating osteoclast cultures, primary bone marrow cells from 6–10-wk-old mice were cultured as described previously (Fuller et al., 2000) in 20 ng/ml M-CSF and 5 ng/ml RANKL (R&D Systems) for 6 d on plastic or for 7 d on cortical bovine bone slices (provided by O. Hoffmann, University of Vienna, Vienna, Austria), or in 20 ng/ml M-CSF on plastic for proliferation analyses of preosteoclasts. To test resorptive activity on bone slices, culture medium was acidified to pH ∼7.0 for the last 2 d of culture to activate resorption. Resorption pits were stained with toluidine blue. Co-culture experiments with primary osteoblasts were performed as described previously (Jochum et al., 2000).

Microscopic analysis of osteoblast and osteoclast cultures was performed using a stereomicroscope (MZ-Apo; Leica) with Plan-Apo 1.0× lenses. The images were recorded using a CCD camera (DKC-5000; Sony) using ImageAccess software (Imagic).

For BrdU incorporation, BrdU was added to the last 2 h (osteoblasts) or 6 h (M-CSF–treated osteoclast precursors) of proliferating cultures to a final concentration of 10 mM. Cells were immunostained with anti-BrdU antibody (Abcam) according to standard procedures. In situ nick end-labeling (TUNEL) was performed using the in situ cell death detection kit II (Boehringer).

For analysis of synchronized osteoblasts, cells were cultured for 1 d and thereafter serum-starved. After 48 h, MEM with 15% FCS was added and osteoblasts were analyzed at 0-, 4-, and 8-h time points. For FACS® analysis for cell cycle profiling of proliferating osteoblasts, BrdU was added at restimulation and osteoblasts were fixed in 85% ethanol. All cell culture assays were performed at least two times (mostly three times), with four replicates per experiment.

Statistics

Statistical analysis was performed using *t* test; $P < 0.05$ was accepted as significant. Error bars represent the SD.

We thank Hans Christian Theussl for blastocyst injections, Hannes Tkad-

letz for help with the illustrations, Latifa Bakiri for helpful discussions, M. Yaniv for providing us with JunB antibody, Arndt Schilling for help with μCT analysis, Matthias Priemel for blinded interobserver control of quantitative histomorphometry, Sylvia Schauer for preparing histological sections, Martina Rath for technical assistance, Oskar Hoffmann for providing us with bovine bone discs, and Christine Hartmann for providing us with ISH probes. We also thank Agi Grigoriadis, Christine Hartmann, and Jochen Hess for critical reading of the manuscript.

The IMP is funded by Boehringer Ingelheim, and this work was supported by the Austrian Industrial Research Promotion Fund, the Deutsche Forschungsgemeinschaft (SCHO 365/3-1), and by the BioMed-2 and Training and Mobility of Researchers. A. Hoebertz was the recipient of awards from the European Molecular Biology Organization and from Marie-Curie Individual Fellowships.

Submitted: 28 August 2003
Accepted: 23 December 2003

References

Amling, M., M. Priemel, T. Holzmann, K. Chapin, J.M. Rueger, R. Baron, and M.B. Demay. 1999. Rescue of the skeletal phenotype of vitamin D receptor-ablated mice in the setting of normal mineral ion homeostasis, formal histomorphometric and biomechanical analyses. *Endocrinology.* 140: 4982–4987.

Amling, M., L. Neff, M. Priemel, A.F. Schilling, J.M. Rueger, and R. Baron. 2000. Progressive increase in bone mass and development of odontomas in aging osteopetrotic c-src-deficient mice. *Bone.* 27:603–610.

Andrecht, S., A. Kolbus, B. Hartenstein, P. Angel, and M. Schorpp-Kistner. 2002. Cell cycle promoting activity of JunB through cyclin A activation. *J. Biol. Chem.* 277:35961–35968.

Aslam, F., L. McCabe, B. Frenkel, A.J. van Wijnen, G.S. Stein, J.B. Lian, and J.L. Stein. 1999. AP-1 and vitamin D receptor (VDR) signaling pathways converge at the rat osteocalcin VDR element: requirement for the internal activating protein-1 site for vitamin D-mediated trans-activation. *Endocrinology.* 140:63–70.

Bakiri, L., D. Lallemand, E. Bossy-Wetzel, and M. Yaniv. 2000. Cell cycle-dependent variations in c-Jun and JunB phosphorylation: a role in the control of cyclin D1 expression. *EMBO J.* 19:2056–2068.

Behrens, A., J. Haigh, F. Mechta-Grigoriou, A. Nagy, M. Yaniv, and E.F. Wagner. 2003. Impaired intervertebral disc formation in the absence of Jun. *Development.* 130:103–109.

Chiu, R., P. Angel, and M. Karin. 1989. Jun-B differs in its biological properties from, and is a negative regulator of, c-Jun. *Cell.* 59:979–986.

Clausen, B.E., C. Burkhardt, W. Reith, R. Renkawitz, and I. Forster. 1999. Conditional gene targeting in macrophages and granulocytes using LysMcre mice. *Transgenic Res.* 8:265–277.

Corrall, D.A., M. Amling, M. Priemel, E. Loyer, S. Fuchs, P. Ducy, R. Baron, and G. Karsenty. 1998. Dissociation between bone resorption and bone formation in osteopenic transgenic mice. *Proc. Natl. Acad. Sci. USA.* 95:13835–13840.

David, J.P., M. Rincon, L. Neff, W.C. Horne, and R. Baron. 2001. Carbonic anhydrase II is an AP-1 target gene in osteoclasts. *J. Cell. Physiol.* 188:89–97.

David, J.P., K. Sabapathy, O. Hoffmann, M.H. Idarraga, and E.F. Wagner. 2002. JNK1 modulates osteoclastogenesis through both c-Jun phosphorylation-dependent and -independent mechanisms. *J. Cell Sci.* 115:4317–4325.

Ducy, P., R. Zhang, V. Geoffroy, A.L. Ridall, and G. Karsenty. 1997. Osf2/Cbfa1: a transcriptional activator of osteoblast differentiation. *Cell.* 89:747–754.

Ducy, P., M. Starbuck, M. Priemel, J. Shen, G. Pinero, V. Geoffroy, M. Amling, and G. Karsenty. 1999. A Cbfa1-dependent genetic pathway controls bone formation beyond embryonic development. *Genes Dev.* 13:1025–1036.

Eferl, R., and E.F. Wagner. 2003. AP-1: a double-edged sword in tumorigenesis. *Nat. Rev. Cancer.* 3:859–868.

Eferl R., M. Sibilia, F. Hilberg, A. Fuchsbichler, I. Kufferath, B. Guertl, R. Zenz, E.F. Wagner, and K. Zatloukal. 1999. Functions of c-Jun in liver and heart development. *J. Cell Biol.* 145:1049–1061.

Fuller, K., J.M. Lean, K.E. Bayley, M.R. Wani, and T.J. Chambers. 2000. A role for $TGF\beta_1$ in osteoclast differentiation and survival. *J. Cell Sci.* 113:2445–2453.

Grigoriadis, A.E., K. Schellander, Z.Q. Wang, and E.F. Wagner. 1993. Osteoblasts are target cells for transformation in c-fos transgenic mice. *J. Cell Biol.* 122: 685–701.

Grigoriadis, A.E., Z.Q. Wang, M.G. Cecchini, W. Hofstetter, R. Felix, H.A. Fleisch, and E.F. Wagner. 1994. c-Fos: a key regulator of osteoclast-macrophage lineage determination and bone remodeling. *Science.* 266:443–448.

Hess, J., B. Hartenstein, S. Teurich, D. Schmidt, M. Schorpp-Kistner, and P. Angel. 2003. Defective endochondral ossification in mice with strongly compromised expression of JunB. *J Cell Sci.* 15:4587–4596.

Jochum, W., J.P. David, C. Elliott, A. Wutz, H. Plenk, Jr., K. Matsuo, and E.F. Wagner. 2000. Increased bone formation and osteosclerosis in mice overexpressing the transcription factor Fra-1. *Nat. Med.* 6:980–984.

Jochum, W., E. Passegue, and E.F. Wagner. 2001. AP-1 in mouse development and tumorigenesis. *Oncogene.* 20:2401–2412.

Karsenty, G., and E.F. Wagner. 2002. Reaching a genetic and molecular understanding of skeletal development. *Dev. Cell.* 2:389–406.

Komori, T., H. Yagi, S. Nomura, A. Yamaguchi, K. Sasaki, K. Deguch, Y. Shimizu, R.T. Bronson, Y.H. Gao, M. Inada, et al. 1997. Targeted disruption of Cbfa1 results in a complete lack of bone formation owing to maturational arrest of osteoblasts. *Cell.* 89:755–764.

Liu, W., S. Toyosawa, T. Furuichi, N. Kanatani, C. Yoshida, Y. Liu, M. Himeno, S. Narai, A. Yamaguchi, and T. Komori. 2001. Overexpression of Cbfa1 in osteoblasts inhibits osteoblast maturation and causes osteopenia with multiple fractures. *J. Cell Biol.* 155:157–166.

Malaval, L., F. Liu, P. Roche, and J.E. Aubin. 1999. Kinetics of osteoprogenitor proliferation and osteoblast differentiation in vitro. *J. Cell. Biochem.* 74:616–627.

Matsuo, K., J.M. Owens, M. Tonko, C. Elliott, T.J. Chambers, and E.F. Wagner. 2000. Fosl1 is a transcriptional target of c-Fos during osteoclast differentiation. *Nat. Genet.* 24:184–187.

McCabe, L.R., M. Kockx, J. Lian, J. Stein, and G. Stein. 1995. Selective expression of fos- and jun-related genes during osteoblast proliferation and differentiation. *Exp. Cell Res.* 218:255–262.

Murtaugh, L.C., J.H. Chyung, and A.B. Lassar. 1999. Sonic hedgehog promotes somitic chondrogenesis by altering the cellular response to BMP signaling. *Genes Dev.* 13:225–237.

Parfitt, A.M., M.K. Drezner, F.H. Glorieux, J.A. Kanis, H. Malluche, P.J. Meunier, S.M. Ott, and R.R. Recker. 1987. Bone histomorphometry: standardization of nomenclature, symbols, and units. Report of the ASBMR Histomorphometry Nomenclature Committee. *J. Bone Miner. Res.* 2:595–610.

Passegue, E., and E.F. Wagner. 2000. JunB suppresses cell proliferation by transcriptional activation of p16 (INK4a) expression. *EMBO J.* 19:2969–2979.

Passegue, E., W. Jochum, M. Schorpp-Kistner, U. Mohle-Steinlein, and E.F. Wagner. 2001. Chronic myeloid leukemia with increased granulocyte progenitors in mice lacking junB expression in the myeloid lineage. *Cell.* 104:21–32.

Passegue, E., W. Jochum, A. Behrens, R. Ricci, and E.F. Wagner. 2002. JunB can substitute for Jun in mouse development and cell proliferation. *Nat. Genet.* 30:158–166.

Sabatakos, G., N.A. Sims, J. Chen, K. Aoki, M.B. Kelz, M. Amling, Y. Bouali, K. Mukhopadhyay, K. Ford, E.J. Nestler, and R. Baron. 2000. Overexpression of ΔFosB transcription factor(s) increases bone formation and inhibits adipogenesis. *Nat. Med.* 6:985–990.

Schorpp, M., R. Jager, K. Schellander, J. Schenkel, E.F. Wagner, H. Weiher, and P. Angel. 1996. The human ubiquitin C promoter directs high ubiquitous expression of transgenes in mice. *Nucleic Acids Res.* 24:1787–1788.

Schorpp-Kistner, M., Z.Q. Wang, P. Angel, and E.F. Wagner. 1999. JunB is essential for mammalian placentation. *EMBO J.* 18:934–948.

Shaulian E., and M. Karin. 2002 AP-1 as a regulator of cell life and death. *Nat. Cell Biol.* 4:E131–E136.

Simon, C., M. Simon, G. Vucelic, M.J. Hicks, P.K. Plinkert, A. Koitschev, and H.P. Zenner. 2001. The p38 SAPK pathway regulates the expression of the MMP-9 collagenase via AP-1-dependent promoter activation. *Exp. Cell Res.* 271:344–355.

Takayanagi, H., S. Kim, T. Koga, H. Nishina, M. Isshiki, H. Yoshida, A. Saiura, M. Isobe, T. Yokochi, J. Inoue, et al. 2002. Induction and activation of the transcription factor NFATc1 (NFAT2) integrate RANKL signaling in terminal differentiation of osteoclasts. *Dev. Cell.* 3:889–901.

Tallquist, M.D., and P. Soriano. 2000. Epiblast-restricted Cre expression in MORE mice: a tool to distinguish embryonic vs. extra-embryonic gene function. *Genesis.* 26:113–115.

Thepot D., J.B. Weitzman, J. Barra, D. Segretain, M.G. Stinnakre, C. Babinet, and M. Yaniv. 2000. Targeted disruption of the murine junD gene results in multiple defects in male reproductive function. *Development* 127:143–153.

Wisdom, R., R.S. Johnson, and C. Moore. 1999. c-Jun regulates cell cycle progression and apoptosis by distinct mechanisms. *EMBO J.* 18:188–197.

Yamauchi, M., Y. Ogata, R.H. Kim, J.J. Li, L.P. Freedman, and J. Sodek. 1996. AP-1 regulation of the rat bone sialoprotein gene transcription is mediated through a TPA response element within a glucocorticoid response unit in the gene promoter. *Matrix Biol.* 15:119–130.